# Abel inversion of deflectometric data: comparison of accuracy and noise propagation of existing techniques

Pankaj S. Kolhe and Ajay K. Agrawal*

Department of Mechanical Engineering, University of Alabama, Tuscaloosa, Alabama 35487, USA

*Corresponding author: aagrawal@eng.ua.edu

Received 6 April 2009; revised 1 June 2009; accepted 15 June 2009;
posted 17 June 2009 (Doc. ID 109732); published 1 July 2009

Abel inverse integral to obtain local field distributions from path-integrated measurements in an axisymmetric medium is an ill-posed problem with the integrant diverging at the lower integration limit. Existing methods to evaluate this integral can be broadly categorized as numerical integration techniques, semianalytical techniques, and least-squares whole-curve-fit techniques. In this study, Simpson's 1/3rd rule (a numerical integration technique), one-point and two-point formulas (semianalytical techniques), and the Guass–Hermite product polynomial method (a least-squares whole-curve-fit technique) are compared for accuracy and error propagation in Abel inversion of deflectometric data. For data acquired at equally spaced radial intervals, the deconvolved field can be expressed as a linear combination (weighted sum) of measured data. This approach permits use of the uncertainty analysis principle to compute error propagation by the integration algorithm. Least-squares curve-fit techniques should be avoided because of poor inversion accuracy with large propagation of measurement error. The two-point formula is recommended to achieve high inversion accuracy with minimum error propagation. 

*OCIS codes:* 000.2190, 100.6950, 120.5820, 280.1740, 280.2490.

## 1. Introduction

Nonintrusive diagnostics typically consist of local techniques that measure a quantity at a point, plane, or volume, and line-of-sight techniques measuring a chordally integrated quantity. The latter techniques require a deconvolution approach to reconstruct the local field from measurements of the integrated quantity. For an axisymmetric medium, Abel inversion [1] formulas are used to reconstruct the field variable from its one-dimensional projections. Past studies have generally focused on Abel formulas for phase measurements, given as

$$P(x) = 2\int_x^R \frac{f(r)r}{\sqrt{r^2 - x^2}}\,\mathrm{d}r, \tag{1}$$

The Abel inversion integral transform of Eq. (1) is given as

$$f(r) = -\frac{1}{\pi}\int_r^R \frac{\mathrm{d}P(x)}{\mathrm{d}x}\frac{\mathrm{d}x}{\sqrt{x^2 - r^2}}. \tag{2}$$

Equations (1) and (2) find applications in radio astronomy [2], atomic and molecular scattering [3], measurements by spectroscopy (flame/plasma) [4–8], photoelectron imaging experiments [9], combustion and fluid-flow measurements by interferometry [10–12], x-ray radiography [13], optical-fiber refractive-index measurements [14,15], and spray-droplet studies [16]. The integral in Eq. (2) requires differentiation of measured data, which can amplify the measurement error in $P(x)$.

In the present study, we are dealing with Abel formulas for deflectometric measurements. For example, the transverse deflection angle of a ray in a schlieren setup is given by Eq. (3):

0003-6935/09/203894-09$15.00/0

$$\Theta(x) = 2x \int_x^R \frac{\partial \delta}{\partial r} \frac{\mathrm{d}r}{\sqrt{r^2 - x^2}}. \quad (3)$$

The field variable is the normalized refractive-index difference [$\delta = (\eta/\eta_0 - 1)$) where $\eta$ is the local refractive index and $\eta_0$ is the refractive index of the surrounding] obtained from an Abel inverse integral transform of Eq. (3), given as

$$\delta(r) = -\frac{1}{\pi} \int_r^R \Theta(x) \frac{\mathrm{d}x}{\sqrt{x^2 - r^2}}. \quad (4)$$

Equations (3) and (4) are used with measurements obtained by moiré deflectometry [17,18], laser speckle photography [19], and rainbow schlieren deflectometry [20–25], among others. The integral in Eq. (4) is improper with the integrant diverging at the lower integration limit. Moreover, deflection angle measurements will inevitably contain experimental uncertainties or noise. Thus, the procedure to evaluate the integral in Eq. (4) is important from perspectives of accuracy and propagation of measurement uncertainties even though the computational effort is insignificant. The primary objective of the present work is to compare different methods proposed in the literature so that the best approach to evaluate the integral in Eq. (4) can be identified.

Existing algorithms to evaluate local field distribution using either Eq. (2) or Eq. (4) can be categorized as:

1. numerical integration techniques using piecewise curve fitting of the diverging integrant in the Abel integral transform (namely, trapezoidal integration, Simpson's 1/3rd rule, quadrature methods, etc.), [6,26–28].
2. data approximation techniques,

a. semianalytical techniques using piecewise approximation (namely, Lagrangian polynomials, Taylor series expansion) of measured data in each segment evaluated analytically [29–33], or

b. least squares approximation of entire data set or whole-field curve-fit methods (namely, use of Fourier series, orthogonal polynomials, Hermite polynomials, etc.) coupled with analytical integration of the curve-fit function [5,12,14,34].

Most of the studies in each category are similar in theme and they typically present a specific technique without a comparative account of different methods. Cremers and Birkebak [4] compared different techniques based on piecewise approximation of data. Minerbo and Levy [10] presented a method to account for error/uncertainty in the inversion process and used it to systematically compare different polynomials for data approximation. Dasch [30] compared semianalytical techniques to integrate the Abel inverse transform in Eq. (2) and showed, for the first time, that all of the techniques could be cast into linear operator form in Eq. (5):

$$f(r_i) = \frac{1}{\Delta r} \cdot \sum_{j=i}^{\infty} D_{ij} \cdot P_j \quad (5)$$

Dasch [30] used Eq. (5) as a benchmark to compare inversion accuracy and noise propagation behavior of several semianalytical techniques. Past studies deal with phase measurements and, to date, a quantitative assessment of techniques to evaluate Abel integral with deflectometric measurements [Eq. (4)] has not been conducted to the best of our knowledge.

Past investigators have employed two different methods to account for noise propagation. In the first method, input data are infiltrated with noise to determine its propagation during the inversion process [35]. The second method is the typical uncertainty analysis, determining how a known uncertainty in measured data [given in terms of standard deviation or root mean square (RMS)] propagates into uncertainty in a local or inverted quantity [36,37]. However, none of these investigators compared error propagation for inversion techniques of different categories listed above (namely, numerical integration, semianalytical integration, and least-squares approximation).

In this study, four different techniques to evaluate the Abel inversion integral in Eq. (4) are presented. It is shown that each of these techniques can be expressed in a linear operator form similar to that employed by Dasch [30]. This feature allows comparison of different techniques using the standard error propagation analysis procedure. While all of these methods are remarkably similar and the computational effort is less than 1 min on a personal computer, the semianalytical technique using piecewise approximation by a linear profile is found to be superior to other techniques in terms of both accuracy and propagation of measurement error.

## 2. Inversion Algorithms

The algorithms addressed in this study are

1. numerical integration using Simpsons' 1/3rd rule,
2. a semianalytical technique with piecewise approximation in a segment by a constant profile (one-point formula),
3. a semianalytical technique with piecewise approximation in a segment by a linear profile (two-point formula), and
4. a least-squares approximation of a dataset using the Guass–Hermite product polynomial (GHPP).

These techniques to evaluate the integral in Eq. (4) are compared assuming that the line-of-sight deflection angle data are available at equally spaced intervals ($N$ segments). Following Dasch [30], all of these techniques can be recast in the following form:

$$\delta(r_i) = \sum_{j=i}^{N+1} D_{ij} \cdot \Theta_j. \quad (6)$$

Here $\Theta(r_j)$ represents the deflection angle data at spacing of $\Delta r$, $\delta(r_j)$ is the discrete refractive-index difference field, and $r_j = (j-1).\Delta r$ is the radial distance. Here $i$ and $j$ are indices corresponding to data points varying from 1 to $N+1$. The linear operator coefficients $D_{ij}$ are independent of the data spacing $\Delta r$ except for in the GHPP method. Nevertheless, $D_{ij}$ coefficients can be determined *a priori* for each inversion algorithm. The procedure to recast inversion techniques in the form of Eq. (6) is discussed in the following.

### A. Simpson's 1/3rd Rule

The Simpson's 1/3rd rule applied to discretized form of Eq. (4) results in Eq. (7a):

$$\delta(r_i) = \frac{-1}{\pi}\int_{r_i}^{R}\frac{\Theta(r)\mathrm{d}r}{\sqrt{r^2-r_i^2}} = \frac{-1}{\pi}\sum_{j=i,\mathrm{incr}=2}^{N-1}\int_{r_j}^{r_{j+2}}\frac{\Theta(r_j)\mathrm{d}r_j}{\sqrt{r_j^2-r_i^2}}$$
$$= \frac{-1}{\pi}\sum_{j=i,\mathrm{incr}=2}^{N-1}\left[\frac{\Delta r}{3}\cdot\left(\frac{\Theta_j}{\sqrt{r_j^2-r_i^2}}+\frac{4\Theta_{j+1}}{\sqrt{r_{j+1}^2-r_i^2}}+\frac{\Theta_{j+2}}{\sqrt{r_{j+2}^2-r_i^2}}\right)\right]. \tag{7a}$$

Equation (7a) can be recast in the form of Eq. (6), where

$$\mathrm{D_{ij}} = \frac{-1}{3\pi}\cdot\frac{\left[2+\left(1+(-1)^{(j-i+1)}\right)\right]}{\sqrt{(j-1)^2-(i-1)^2}} \quad \text{if } j>i \quad \text{and} \quad j\neq N+1,$$
$$= \frac{-1}{3\pi}\cdot\frac{\left[2+\left(1+(-1)^{(j-i+1)}\right)\right]}{2\cdot\sqrt{(j-1)^2-(i-1)^2}} \quad \text{if } j=N+1,$$
$$= 0 \quad \text{if } j<i. \tag{7b}$$

The singularity at $j=i$ is eliminated by extrapolating from remaining $D_{ij}$ coefficients, as shown in Eq. (7c):

$$D_{ii} = D_{i(i+1)} \quad \text{for } i\le N, \qquad = 0 \quad \text{for } i = N+1. \tag{7c}$$

### B. One-Point Formula

One-Point formulation is quite similar to trapezoidal integration with the difference that, instead of the complete integrand in Eq. (4), which results in singularity at $x=r$, the deflection angle in each segment is represented by a constant profile. The resulting integrand for each segment is then solved analytically. Thus,

$$\delta(r) = -\frac{1}{\pi}\cdot\int_r^{\infty}\Theta(x)\cdot\frac{\mathrm{d}x}{\sqrt{x^2-r^2}}$$
$$= -\frac{1}{\pi}\cdot\sum_{j=1}^{N}\left(\int_0^{\Delta r}\left(\frac{\Theta_j+\Theta_{j+1}}{2}\right)\cdot\frac{\mathrm{d}l}{\sqrt{(r_j+l)^2-r_i^2}}\right), \tag{8}$$

Here the deflection angle is constant over a segment and it is computed as the average of the two neighboring data points. Note that $l$ is the width of the segment. Substituting $r_j = (j-1)\cdot\Delta r$ and $r_i = (i-1)\cdot\Delta r$, Eq. (8) reduces to

$$\delta(r_i) = -\frac{1}{\pi}\cdot\sum_{j=1}^{N}\left(\int_0^{1}\left(\frac{\Theta_j+\Theta_{j+1}}{2}\right)\cdot\frac{\mathrm{d}\beta}{\sqrt{((j-1)+\beta)^2-(i-1)^2}}\right), \tag{9a}$$

where $\beta = \frac{l}{\Delta r}$. After analytical integration, Eq. (9a) can be recast in the form of Eq. (6), where

$$D_{ij} = \frac{-1}{2\pi}\cdot\ln\left(\frac{j+\sqrt{j^2-(i-1)^2}}{(j-2)+\sqrt{(j-2)^2-(i-1)^2}}\right) \quad \text{if } j>i \quad \text{and} \quad j\neq 2,$$
$$= \frac{-1}{2\pi}\cdot\left(2+\ln\left(\frac{j+\sqrt{j^2-(i-1)^2}}{(j-1)+\sqrt{(j-1)^2-(i-1)^2}}\right)\right) \quad \text{if } j>i \quad \text{and} \quad j=2,$$
$$= \frac{-1}{2\pi}\cdot\ln\left(\frac{j+\sqrt{j^2-(i-1)^2}}{(j-1)+\sqrt{(j-1)^2-(i-1)^2}}\right) \quad \text{if } j=i \quad \text{and} \quad i\neq 1,$$
$$= 0 \quad \text{if } j<i \quad \text{or} \quad j=i=1. \tag{9c}$$

The analytical integral in Eq. (9a) is undefined in the first segment, where the deflection angle is assumed to vary linearly to yield $D_{i=1j=1} = 0$.

### C. Two-Point Formula

The two-point formula follows the same procedure as the one-point formula except that the deflection angle is approximated by a linear profile in each segment. Thus, Eq. (4) results in the following approximation:

$$\delta(r) = -\frac{1}{\pi}\cdot\int_{r}^{\infty}\Theta(x)\cdot\frac{\mathrm{d}x}{\sqrt{x^2-r^2}}$$
$$= -\frac{1}{\pi}\cdot\sum_{j=1}^{N}\left(\int_{0}^{\Delta r}\left(\Theta_j + l\cdot\frac{(\Theta_{j+1}-\Theta_j)}{\Delta r}\right)\cdot\frac{\mathrm{d}l}{\sqrt{(r_j+l)^2-r_i^2}}\right). \quad (10a)$$

After analytical integration, Eq. (10a) can be recast in the form of Eq. (6), where

$$D_{ij} = \frac{1}{\pi}\cdot(A_{i,j} - A_{i,(j-1)} - j\cdot B_{i,j} + (j-2)\cdot B_{i,(j-1)})$$
$$\text{if } j > i \quad \text{and} \quad j \neq 2,$$
$$= \frac{1}{\pi}\cdot(A_{i,j} - j\cdot B_{i,j} - 1) \quad \text{if } j > i \quad \text{and} \quad j = 2,$$
$$= \frac{1}{\pi}\cdot(A_{i,j} - j\cdot B_{i,j}) \quad \text{if } j = i \quad \text{and} \quad i \neq 1,$$
$$= 0 \quad \text{if } j = i = 1 \text{ or } j < i \quad (10b)$$

$$A_{i,j} = \sqrt{j^2-(i-1)^2} - \sqrt{(j-1)^2-(i-1)^2},$$
$$B_{i,j} = \ln\left(\frac{j+\sqrt{j^2-(i-1)^2}}{(j-1)+\sqrt{(j-1)^2-(i-1)^2}}\right). \quad (10c)$$

### D. Gauss–Hermite Product Polynomial Method

In this method, wherein the deflection angle data are represented by the product of Gaussian and Hermite polynomials with the first seven odd polynomials, i.e., the 13th-order polynomial is the highest-order polynomial [34],

$$\Theta(x) = \left(\sum_{p=0}^{6} a_{(2p+1)}\cdot\sum_{q=0}^{6} H_{(2p+1),(2q+1)}\cdot y^{(2q+1)}\right)\cdot e^{-x^2}. \quad (11)$$

Substituting Eq. (11) into the discrete form of Eq. (4), we obtain

$$\delta(r_i) = \frac{-1}{\pi}\cdot\int_{r_i}^{\infty}\frac{\Theta(x)\cdot\mathrm{d}x}{\sqrt{x^2-r_i^2}}$$
$$= \frac{-1}{\pi}\cdot\int_{r_i}^{\infty}\left(\sum_{p=0}^{6} a_{(2p+1)}\cdot\sum_{q=0}^{6} H_{(2p+1),(2q+1)}\cdot x^{(2q+1)}\right)\cdot e^{-x^2}\cdot\frac{\mathrm{d}x}{\sqrt{x^2-r_i^2}} \Rightarrow \delta(r_i)$$
$$= \frac{-1}{\pi}\cdot\left(\sum_{p=0}^{6} a_{(2p+1)}\cdot\sum_{q=0}^{6} H_{(2p+1),(2q+1)}\cdot I_{q,i}\right), \quad (12)$$

where $I_{q,i} = \int_{r_i}^{\infty} x^{(2q+1)}\cdot\exp(-x^2)\cdot(x^2-r_i^2)^{1/2}\cdot\mathrm{d}x$ has an exact analytical solution as given by Rubinstein and Greenberg [34]. After algebraic manipulation, Eq. (12) can be recast in the form of Eq. (6), where

$$D_{ij} = \frac{-1}{\pi^{3/2}}\cdot\sum_{p=0}^{6}\left(\begin{array}{l}\frac{1}{(2p+1)!\cdot 2^{(2p+1)}}\cdot\sum_{q=0}^{6}\left(\begin{array}{l}H_{(2p+1),(2q+1)}\cdot(j-1)^{(2q+1)}\\ \cdot(\Delta r)^{(2q+2)}\end{array}\right)\\ \cdot\sum_{q=0}^{6} H_{(2p+1),(2q+1)}\cdot I_{q,i}\end{array}\right) \quad \text{if } j = 1 \quad \text{or} \quad N+1,$$
$$= \frac{-1}{\pi^{3/2}}\cdot\sum_{p=0}^{6}\left(\begin{array}{l}\frac{1}{(2p+1)!\cdot 2^{(2p+1)}}\cdot\sum_{q=0}^{6}\left(\begin{array}{l}H_{(2p+1),(2q+1)}\cdot\left(2\cdot(j-1)^{(2q+1)}\right)\\ \cdot(\Delta r)^{(2q+2)}\end{array}\right)\\ \cdot\sum_{q=0}^{6} H_{(2p+1),(2q+1)}\cdot I_{q,i}\end{array}\right) \quad \text{if } 1 < j < N+1. \quad (13a)$$

The above analysis shows that all techniques can be recast in the form of Eq. (6), which can be represented by the matrix equation $\delta = D\cdot\Theta$ where $\delta$ and $\Theta$ are column vectors of length $N+1$ and $D$ is the inversion coefficient matrix of size $(N+1)\times(N+1)$, known *a priori* depending upon the inversion technique.

Figure 1 compares the inversion coefficient ($D_{i=10,j}$) for different algorithms. Results show that the $D_{ij}$ for various inversion techniques are similar and follow an asymptotic trend with increasing radius except for the GHPP method. The inversion coefficients for the GHPP method depend on the data spacing and, hence, the accuracy of inversion is compromised as discussed in Section 3. The asymptotic trend

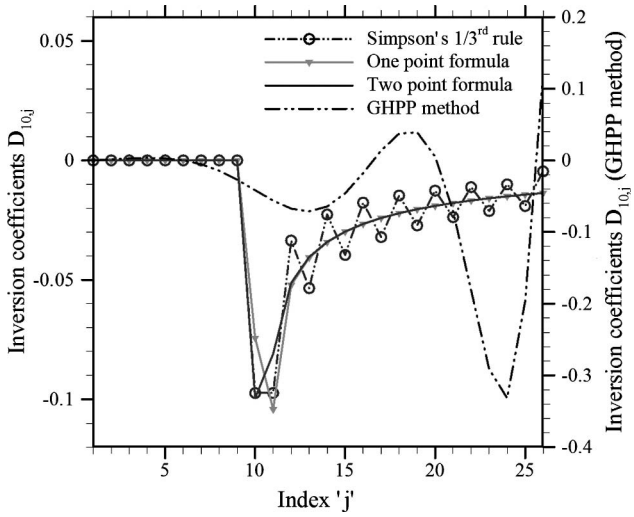


Fig. 1. Comparison of inversion coefficient ($D_{10j}$) for different algorithms ($N = 25$).

signifies diagonal dominance in the inversion coefficient matrix, which means that the regions localized to the point under consideration ($i \approx j$) have greater weight than regions farther away ($j > i$) from it. The GHPP method, however, results in a significantly different inversion coefficient profile. All techniques except the GHPP method result in an upper triangular form of the inversion coefficient matrix, indicating that the interior points ($j < i$) have no effect on the inversion. In contrast, the GHPP method employs a single curve to fit the entire dataset; thus, the inversion coefficient matrix is a full matrix and data on both sides of the point under consideration affect the inversion.

### 3. Inversion Accuracy

In this study, a test profile of refractive-index difference taken as the sum of Gaussian distributions given by Eq. (14) is chosen:

$$\delta(r) = \left(e^{-(r-1)^2} + e^{-(r+1)^2}\right). \tag{14}$$

The corresponding line-of-sight deflection angle data are obtained using a semianalytical numerical integration procedure outlined by Shenoy *et al.* [38]. Integration was carried out with 1000 segments to obtain deflection angle data with high accuracy. However, only 51 equispaced deflection angle data points were used as input to verify the accuracy of the proposed inversion algorithms. Figure 2 shows the refractive-index difference profile and the corresponding deflection angle profile used for algorithm verification.

Figure 3(a) compares refractive-index difference profiles reconstructed using different algorithms discussed previously. Results show that all of the inversion algorithms produce accurate results, except for the GHPP method, which incurs large errors in the center region ($r < 1.0$). The inversion error defined as

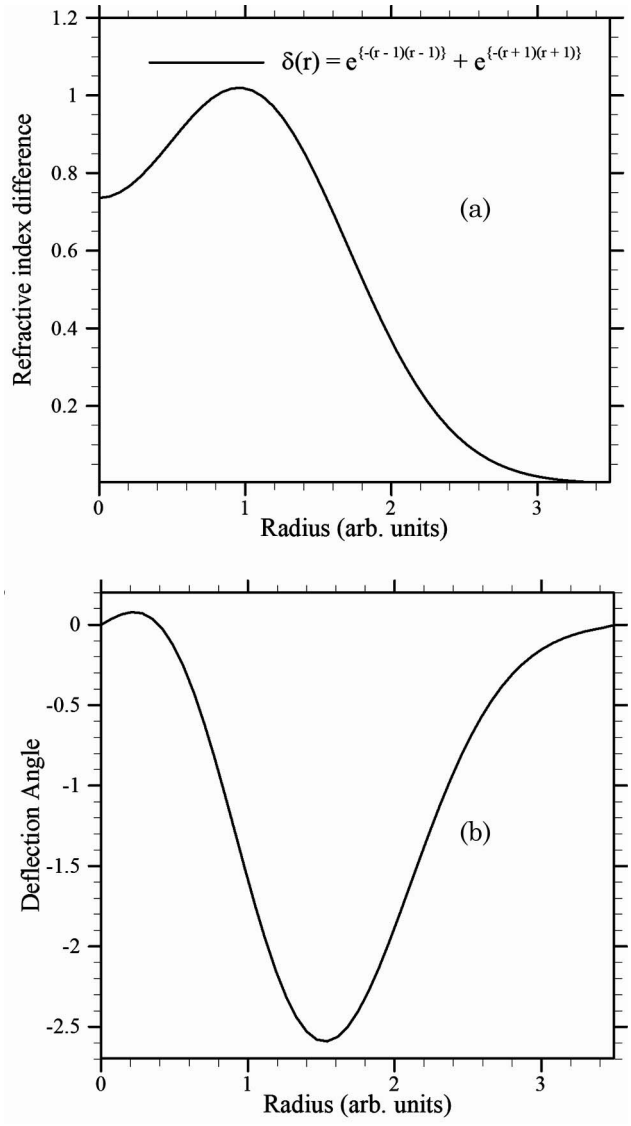


Fig. 2. Test profiles of (a) refractive-index difference (to be reconstructed) and (b) transverse deflection angle (input data).

the difference between the original [Fig. 2(a)] and reconstructed profiles is shown in Fig. 3(b) for all but the GHPP method. Results show the highest inversion error for the Simpson's 1/3rd formula and the least inversion error for the two-point formula. Simpson's 1/3rd rule accuracy was dependent on the treatment of the singularity of the improper integral. The authors investigated open and semiopen extended formulation of the trapezoidal and Simpson's 1/3rd rule [39] to avoid the singularity; however, the inaccuracy in the reconstructed field rendered these treatments unusable.

The GHPP method employs a single curve to fit the entire dataset. Thus, the curve-fit accuracy affects the inversion accuracy. The curve fit is generated from a linear combination of Gauss–Hermite polynomial basis functions varying asymptotically with radius and, hence, they provide accurate curve fit only if data show asymptotic behavior with radius (at

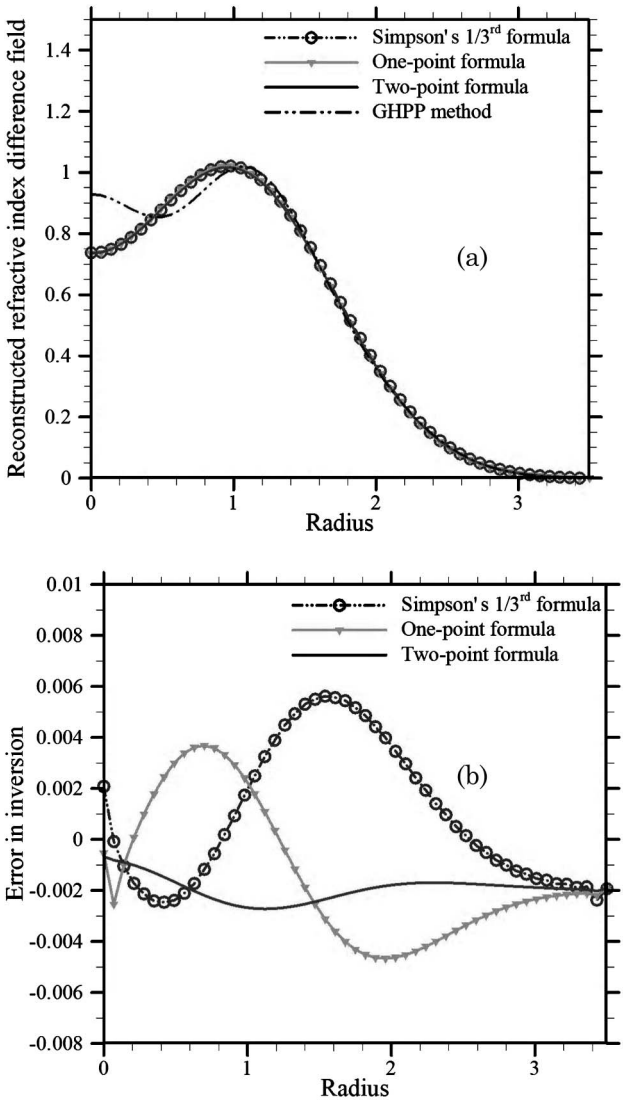


Fig. 3. Inversion accuracy of different algorithms: (a) inverted profile and (b) error in inversion.

$r \approx \pi$). This requirement can be imposed by adding a buffer region (dummy data points) to the profile in Fig. 2(b), such that $\Theta = 0$ for $3.5 < r < 7.0$. Figure 4 shows that the GHPP method with buffer nearly eliminates the curve-fit error in the deflection angle profile. An increase in the number of input data points will, however, increase the computational effort for the GHPP method with buffer.

Figure 5 shows a vast improvement in the inversion accuracy of the GHPP method with buffer such that the inversion error for the GHPP method is similar to that of the two-point formula. Evidently, the reconstruction accuracy of least-squares approximation methods depends largely on the shape of the input profile. The inversion accuracy is higher if the input profile is asymptotic over a sufficiently large region. If experimental data are not asymptotic, dummy data must be appended to improve the inversion accuracy. Methods employing Fourier series or orthogonal polynomials (namely, Laguerre, Hermite,

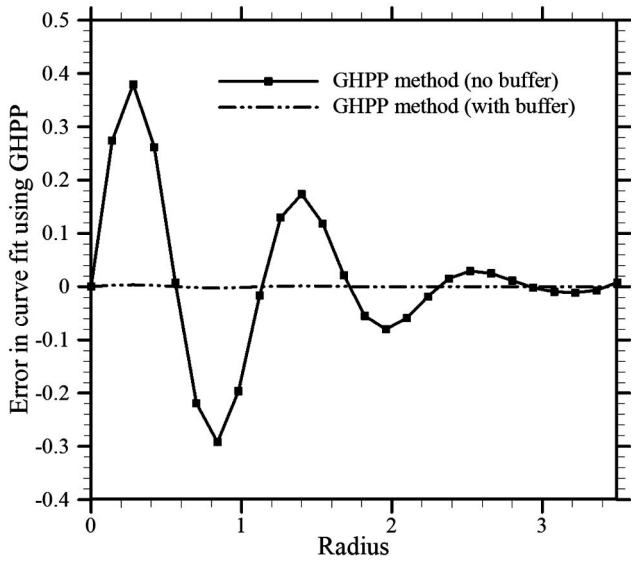


Fig. 4. Effect of buffer zone on curve-fit error using GHPP.

Legendre, Chebyshev, Jacobi, Gegenbauer) to approximate data by least-squares curve fit suffer from a similar drawback and they are accurate only for certain types of input data profiles. GHPP method also has severe drawback if the maximum radius is very small or large. The radial coordinate must be normalized such that the maximum value is around '$\pi$'. The above quantitative comparison supplemented with results for several other input data profiles not shown here, suggests that the two-point formula is by far the best method. GHPP method provides accuracy comparable to two-point method only if input data are buffered and/or the radial coordinate is normalized to maximum value around '$\pi$'.

## 4. Error Propagation

So far, we have considered only a smooth input data set. In practice, however, experimental data would be corrupted by unavoidable random noise in the measurements. Therefore, knowledge of noise damping or magnification in the inversion process is important to assess the reliability of the algorithm. In this study, the well-established uncertainty analysis principle [40] is used to compute the error propagation by the inversion algorithm. The elemental error source is the measurement error at discrete data points. This error source is propagated by the numerical procedure employed to evaluate the Abel integral using the data reduction Eq. (6). Therefore, the total uncertainty in the inverted function is given by

$$U_{\delta(i)} = \sqrt{\sum_{j=i}^{N+1}\left(\left(\frac{\partial}{\partial\Theta_j}\left(\sum_{j=i}^{N+1} D_{ij}\cdot\Theta_j\right)\right)^2 \cdot U_{\Theta_j}^2\right)}$$
$$= \sqrt{\sum_{j=i}^{N+1}(D_{ij}\cdot U_{\Theta_j})^2}, \qquad (15)$$

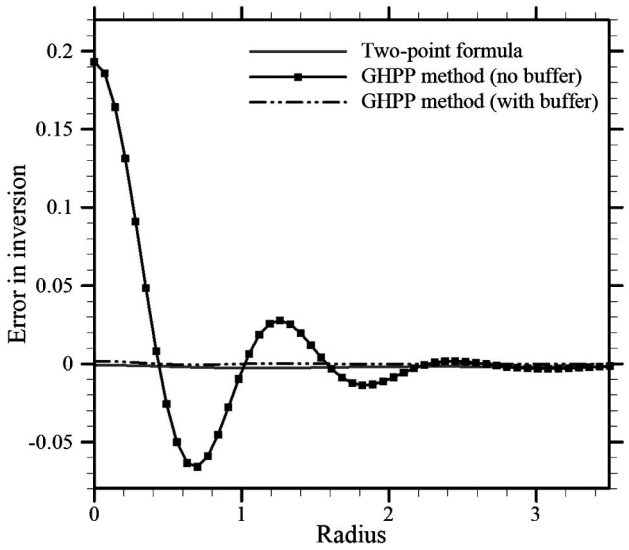


Fig. 5. Inversion error with and without a buffer zone in the GHPP method.

Here, $U_{\delta(i)}$ and $U_{\Theta_j}$ are. respectively. the standard errors in the inverted function (refractive-index difference) and deflectometric measurements. Equation (15) shows that the propagated error is independent of the magnitude of the experimental data and only depends on the standard error profile. Thus, error propagation analysis for various standard error profiles can be performed without the knowledge of the actual deflection angle profile although, in practice, the error profile would depend upon the measured deflection angle profile.

For uniform standard error in input data, $U_{\theta_i} = 1.0$, Figure 6 shows the propagated error, which is highest at the center ($r = 0$) for all of the algorithms. The error propagated for the GHPP method (with buffer) is much larger compared to the other algorithms, of which the two-point formula is the best.

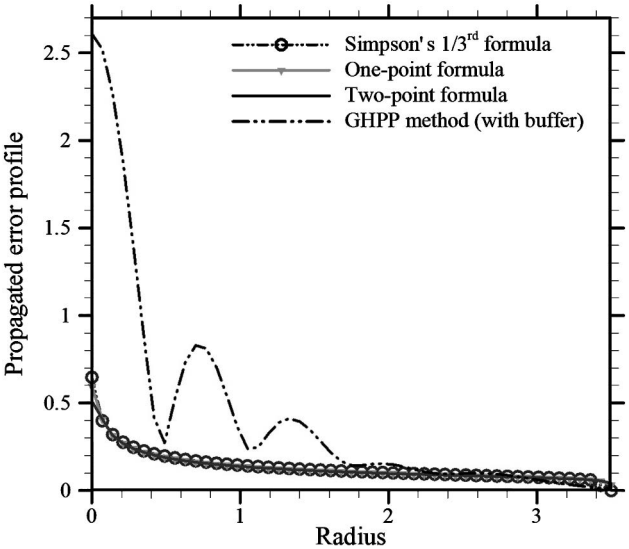


Fig. 6. Error propagation for different algorithms using a uniform error in input data.

For the GHPP method, although the buffer zone improves the inversion accuracy (Fig. 5), it has no effect on the propagation of the measurement error. Figure 7(a) shows a random distribution error profile. The corresponding propagated error profiles for different algorithms are shown in Fig. 7(b). Algorithms other than the GHPP method show a similar trend in error propagation with no clear advantage of one over the other; however, the error amplification of the GHPP method is much larger than all the other algorithms. The maximum propagated error occurs at the center ($r = 0$) for all the algorithms. Figure 8 shows a Gaussian distribution standard error profile and the corresponding error propagation profiles for different algorithms. Again, the error amplification for the GHPP method is much higher compared to the other algorithms. The maximum propagated error location for the GHPP method is at the center whereas, for the other algorithms,

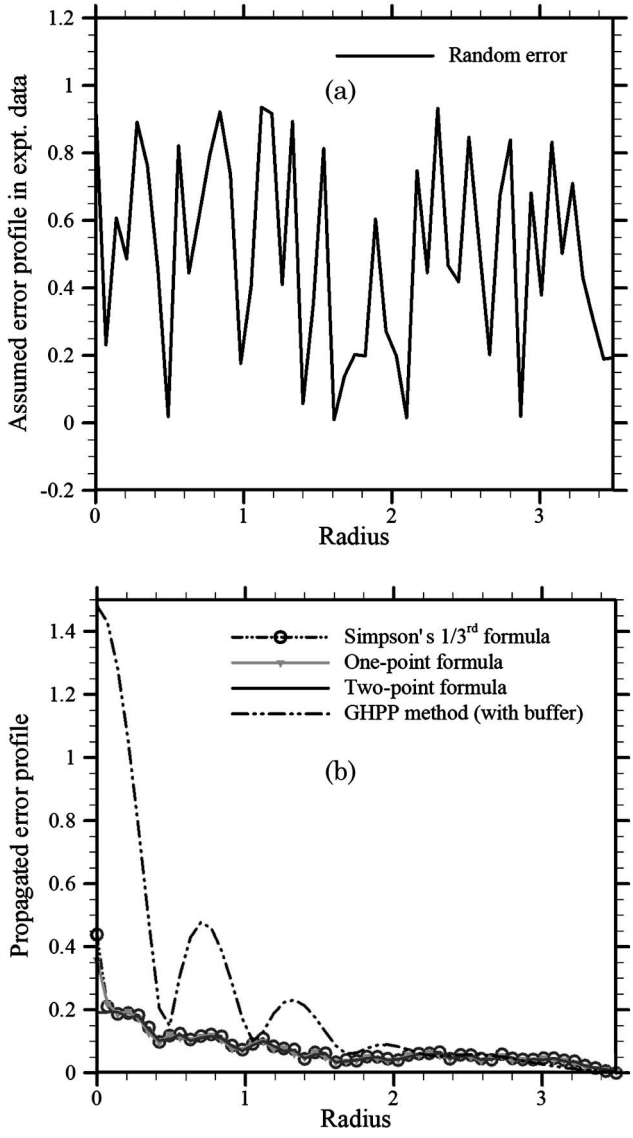


Fig. 7. Error propagation for different algorithms: (a) random error in input data and (b) propagated error profiles.

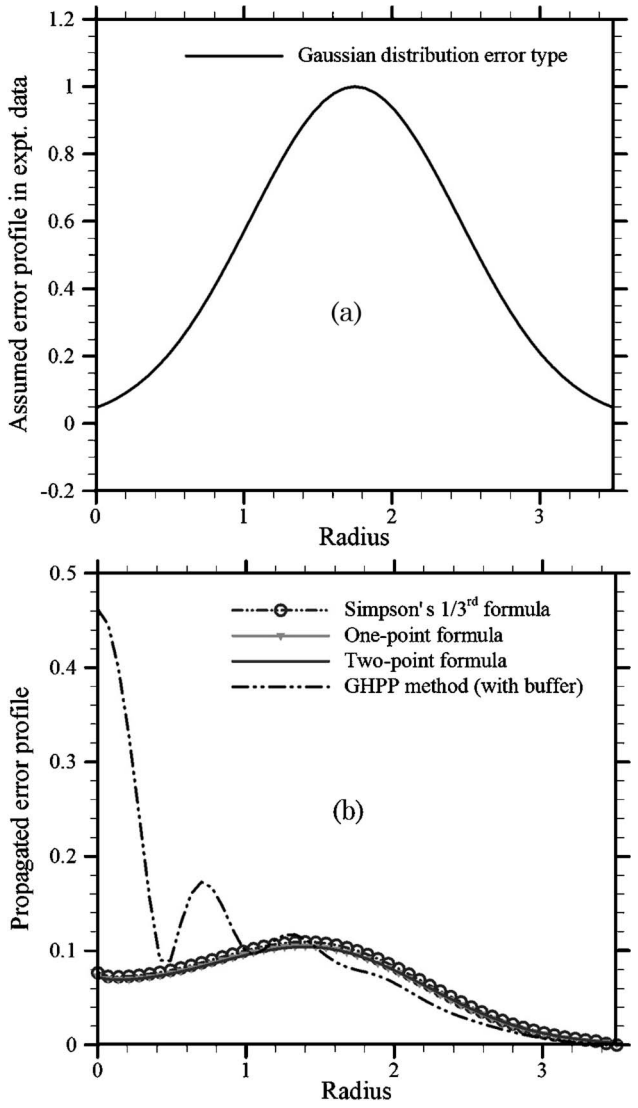


Fig. 8. Error propagation for different algorithms: (a) Gaussian distribution error in input data and (b) propagated error profiles.

the peak propagated error location coincides with the peak in the standard error profile.

## 5. Concluding Remarks

Four Abel inversion techniques using deflectometric measurements are compared for accuracy and propagation of measurement error. These techniques cover existing approaches for Abel inversion and include (1) numerical integration using Simpson's 1/3rd rule, (2) the semianalytical method with piecewise approximation by a constant or linear profile, and (3) least-squares approximation by GHPP. All these methods can be recast in a linear operator form that converts line-of-sight deflection angle data into a local refractive-index difference field. Results show that numerical and semianalytical techniques yield good inversion accuracy, with the two-point formula providing the best accuracy. For the GHPP method, the function value in a segment uniquely determines its values over the entire interval. Thus, this method does not perform well, and it requires a buffer region of dummy data to impose an asymptotic nature in the input data. Error propagation analysis reveals that Simpson's 1/3rd rule, the one-point formula, and the two-point formula perform similarly, although the two-point method is superior. The maximum propagated error location depends on the nature of the standard error input profile for these three methods. The propagated error for the GHPP method is much larger and is unaffected by the buffer zone. Thus, Abel inversion of deflectometric data should be carried out using the two-point formula to achieve high accuracy with minimum propagation of measurement error.

This work was supported in part by the Physical Sciences Division of NASA's Office of Biological and Physical Research under grant NNC05AA36A.

## References

1. N. H. Abel, "Auflosung einer mechanischen Aufgabe," J. Reine Angew. Math. **1**, 153–157 (1826).
2. R. N. Bracewell, "Strip integration in radio astronomy," Aust. J. Phys. **9**, 198–217 (1956).
3. U. Buck, "Inversion of molecular scattering data," Rev. Mod. Phys. **46**, 369–389 (1974).
4. C. J. Cremers and R. C. Birkebak, "Application of the Abel integral equation to spectrographic data," Appl. Opt. **5**, 1057–1064 (1966).
5. M. P. Freeman and S. Katz, "Determination of radial distribution of brightness in a cylindrical luminous medium with self-absorption," J. Opt. Soc. Am. **50**, 826–830 (1960).
6. P. Andanson, B. Cheminat, and A. M. Halbique, "Numerical solution of the Abel integral equation: application to plasma spectroscopy," J. Phys. D Appl. Phys. **11**, 209–215 (1978).
7. K. Bockasten, "Transformation of observed radiances into radial distribution of the emission of a plasma," J. Opt. Soc. Am. **51**, 943–947 (1961).
8. K. M. Green, M. C. Borras, P. P. Woskov, G. J. Flores III, K. Hadidi, and P. Thomas, "Electronic excitation temperature profiles in an air microwave plasma torch," IEEE Trans. Plasma Sci. **29**, 399–406 (2001).
9. V. Dribinski, A. Ossadtchi, V. A. Mandeleshtam, and H. Reisler, "Reconstruction of Abel-transformable images: the Gaussian basis-set expansion Abel transform method," Rev. Sci. Instrum. **73**, 2634–2642 (2002).
10. G. N. Minerbo and M. E. Levy, "Inversion of Abel's integral equation by means of orthogonal polynomials," SIAM J. Numer. Anal. **6**, 598–616 (1969).
11. M. Deutsch and I. Beniaminy, "Inversion of Abel's integral equation for experimental data," J. Appl. Phys. **54**, 137–143 (1983).
12. M. Kalal and K. A. Nugent, "Abel inversion using fast Fourier transforms," Appl. Opt. **27**, 1956–1959 (1988).
13. W. J. Glantschnig and A. Holliday, "Mass fraction profiling based on x-ray tomography and its application to characterizing porous silica boules," Appl. Opt. **26**, 983–989 (1987).
14. K. Tatekura, "Determination of the index profile of optical fibers from transverse interferograms using Fourier theory," Appl. Opt. **22**, 460 (1983).
15. E. Ampem-Lassen, S. T. Huntington, N. M. Dragomir, K. A. Nugent, and A. Roberts, "Refractive index profiling of axially symmetric optical fibers: a new technique," Opt. Express **13**, 3277–3282 (2005).

16. D. C. Hammond, Jr., "Deconvolution technique for line-of-sight optical measurements in axisymmetric sprays," Appl. Opt. **20**, 493–499 (1981).
17. E. Keren, E. Bar-Ziv, I. Glatt, and O. Kafri, "Measurements of temperature distribution of flames by moire deflectometry," Appl. Opt. **20**, 4263–4266 (1981).
18. J. R. Camacho, F. N. Beg, and P. Lee1, "Comparison of sensitivities of Moire deflectometry and interferometry to measure electron densities in z-pinch plasmas," J. Phys. D. **40**, 2026–2032 (2007).
19. P. V. Farrell and D. L. Hofeldt, "Temperature measurement in gases using speckle photography," Appl. Opt. **23**, 1055–1059 (1984).
20. P. S. Greenberg, R. B. Klimek, and D. R. Buchele, "Quantitative rainbow schlieren deflectometry," Appl. Opt. **34**, 3810–3822 (1995).
21. K. Al-Ammar, A. K. Agrawal, S. R. Gollahalli, and D. Griffin, "Concentration measurements in an axisymmetric helium jet using rainbow schlieren deflectometry," Exp. Fluids **25**, 89–95 (1998).
22. A. K. Agrawal, K. N. Alammar, and S. R. Gollahalli, "Application of rainbow schlieren deflectometry to measure temperature and oxygen concentration in a laminar jet diffusion flame," Exp. Fluids **32**, 689–691 (2002).
23. K. S. Pasumarthi and A. K. Agrawal, "Schlieren measurements and analysis of concentration field in self-excited helium jets," Phys. Fluids **15**, 3683–3692 (2003).
24. B. S. Yildirim and A. K. Agrawal, "Full-field concentration measurements of self-excited oscillations in momentum-dominated helium jets," Exp. Fluids **38**, 161–173 (2005).
25. T. Wong and A. K. Agrawal, "Quantitative measurements in an unsteady flame using high-speed rainbow schlieren deflectometry," Meas. Sci. Technol. **17**, 1503–1510 (2006).
26. R. Gorenflo and Y. Kovetz, "Solution of an Abel-type integral equation in the presence of noise by quadratic programming," Numer. Math. **8**, 392–406 (1966).
27. R. Gorenflo and S. Vessella, "Abel integral equations: analysis and applications," in *Lecture Notes in Mathematics*, A. Dold, B. Eckmann, and F. Takens, eds. (Springer-Verlag, 1980).
28. K. E. Atkinson, "The numerical solution of an Abel integral equation by a product trapezoidal method," SIAM J. Numer. Anal. **11**, 97–101 (1974).
29. S. Guerona and M. Deutsch, "A fast Abel inversion algorithm," J. Appl. Phys. **75**, 4313–4318 (1994).
30. C. J. Dasch, "One-dimensional tomography: a comparison of Abel, onion-peeling, and filtered backprojection methods," Appl. Opt. **31**, 1146–1152 (1992).
31. L. A. Vasil'ev, *Schlieren Methods* (Israel Program for Scientific Translations, 1971).
32. O. H. Nestor and H. N. Olson, "Numerical methods for reducing line and surface probe data," SIAM Rev. **2**, 200–207 (1960).
33. W. Frie, "Zur auswertung der Abelschen integralgleichung," Ann. Phys. **465**, 332–339 (1963).
34. R. Rubinstein and P. S. Greenberg, "Rapid inversion of angular deflection data for certain axisymmetric refractive index distributions," Appl. Opt. **33**, 1141–1144 (1994).
35. A. T. Ramsey and M. Diesso, "Abel inversions: error propagation and inversion reliability," Rev. Sci. Instrum. **70**, 380–383 (1999).
36. L. M. Smith, "Nonstationary noise effects in the Abel inversion," IEEE Trans. Inf. Theory **34**, 158–161 (1988).
37. R. K. Paul, J. T. Andrews, K. Bose, and P. K. Barhai, "Reconstruction errors in Abel inversion," Plasma Devices Oper. **13**, 281–290 (2005).
38. A. K. Shenoy, A. K. Agrawal, and S. R. Gollahalli, "Quantitative evaluation of flow computations by rainbow schlieren deflectometry," AIAA J. **36**, 1953–1960 (1998).
39. W. H. Press, S. A. Teukolsky, W. T. Vetterling, and B. P. Flannery, *Numerical Recipes in Fortran: The Art of Scientific Computing*, 2nd ed. (Cambridge U. Press, 1992).
40. H. W. Coleman and W. G. Steele, Jr., *Experimentation and Uncertainty Analysis for Engineers*, 2nd ed. (Wiley, 1999).